AIAA SciTech Forum
12-16 January 2026, Orlando, FL
AIAA SCITECH 2026 Forum

10.2514/6.2026-0278

Effect of a Backward-Facing Step on Drag of a VLEO Satellite

David L. Carroll[1]
CU Aerospace, L.L.C., Champaign, IL, 61822, USA

Keita Nishii[2], Deborah Levin[3]
University of Illinois at Urbana-Champaign, Urbana, IL, 61801, USA

Rodney L. Burton[4], Joseph W. Zimmerman[5], and Ryan T. Fox[6]
CU Aerospace, L.L.C., Champaign, IL, 61822, USA

Spacecraft in very low Earth orbit (VLEO) at altitudes of 150 – 300 km can be prevented from rapid reentry and maintained in orbit with an air-breathing propulsion system that overcomes aerodynamic drag without the need for on-board propellant storage. A conceptual generic satellite shape of an airbreathing VLEO satellite with an electric propulsion thruster and backward-facing step in free molecular flow is presented with a focus on (i) a fundamental examination of drag on a relatively simple vehicle shape, and (ii) fundamental computations for drag and drag reduction on a vehicle shape having a backward-facing step. The magnetoplasmadynamic electric propulsion option is discussed.

I. Nomenclature

B	=	azimuthal magnetic field
CHAOS	=	CUDA-based Hybrid Approach for Octree Simulation
CUDA	=	Compute Unified Device Architecture
c_m	=	most probable random particle speed
DSMC	=	direct simulation Monte Carlo
f	=	pulse frequency
FMF	=	free molecular flow
F_D	=	drag force
g	=	gravitational acceleration
I	=	current
j	=	current density
m	=	mass of gas particles
MPD	=	magnetoplasmadynamic
MPDT	=	magnetoplasmadynamic thruster
n	=	number of DSMC particles
PIC	=	particle in cell
q	=	dynamic pressure $\rho V_{sat}^2/2$
S	=	speed ratio V_{sat}/c_m
U_e	=	exhaust velocity
VLEO	=	very low Earth orbit
V_{sat}	=	satellite orbital velocity

[1] President, Fellow AIAA.
[2] Postdoctoral Research Associate, Aerospace Engineering, Member AIAA.
[3] Professor, Aerospace Engineering, Fellow AIAA.
[4] VP for Research, Associate Fellow AIAA.
[5] Director of Plasmadynamics, Associate Fellow AIAA.
[6] Staff Engineer, Member AIAA.

II. Introduction

A combination of long-established and recent developments in electric propulsion (EP) have opened the probability of allowing continuous orbiting of propellant-less airbreathing satellites in the upper atmosphere, at an altitude of 150 – 300 km at 7.8 km/s and a typical atmospheric density of 1×10^{-9} kg/m^3. Development of the necessary airbreathing propulsion technology would lead to the creation of constellations of small Earth imaging and atmospheric science satellites, allowing the simultaneous orbiting of several satellites on smaller, lower cost booster rockets into a multiplicity of orbits. Recent studies of airbreathing satellites include Tisaev *et al.* [2022], Feldman and Spektor [2022], Crandall and Wirz [2022], Giannetti *et al*. [2024], Herdrich *et al*. [2024], and Burton and Carroll [2025a], among others.

A conceptual generic VLEO satellite design is presented that employs a free molecular flow inlet to admit ram air into a flow compression system to feed an EP thruster system that counteracts drag (**Figure 1**). For the purposes of this fundamental study, a backward-facing step (BFS) results from assuming an EP system in the afterbody with a cross section smaller than the forebody cross section. The effect of the BFS on vehicle drag is discussed here, and a particular electric propulsion option for the generic VLEO satellite is discussed in **Section V**.

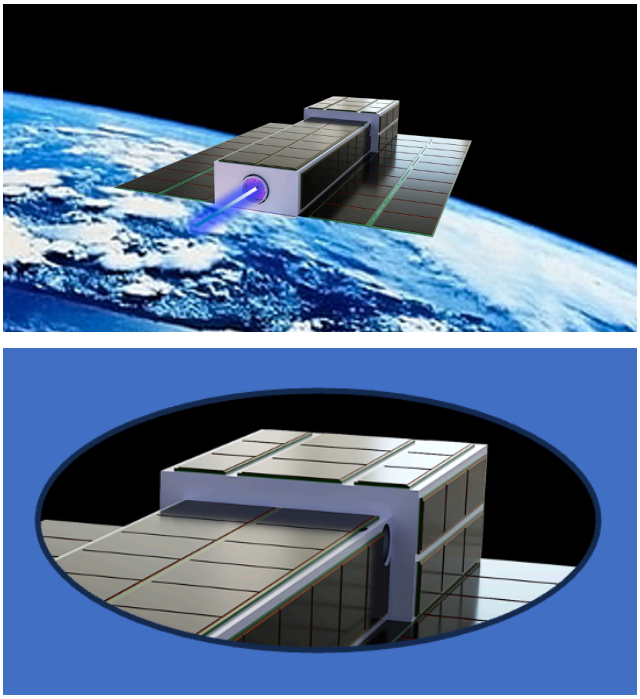

Figure 1. (Top) Rendition of conceptual satellite illustrated from behind the satellite showing afterbody with EP thruster. (Bottom) Magnified image of larger

III. VLEO Satellite with Electric Propulsion

3.1 Conceptual Design

A conceptual design of a VLEO satellite with an EP thruster is illustrated in **Figure 1**. Key features of the layout include: (i) a forebody containing an air inlet and flow compression system, (ii) an afterbody containing the thruster system, and (iii) solar panels which hinge from the base of a full-length rigid exo-frame. The afterbody is smaller in cross section compared to the forebody, which takes advantage of the effective drag reduction for a backward-facing step determined by calculations (see **Section 3.2**). **Figure 2** shows an external illustration of the conceptual design.

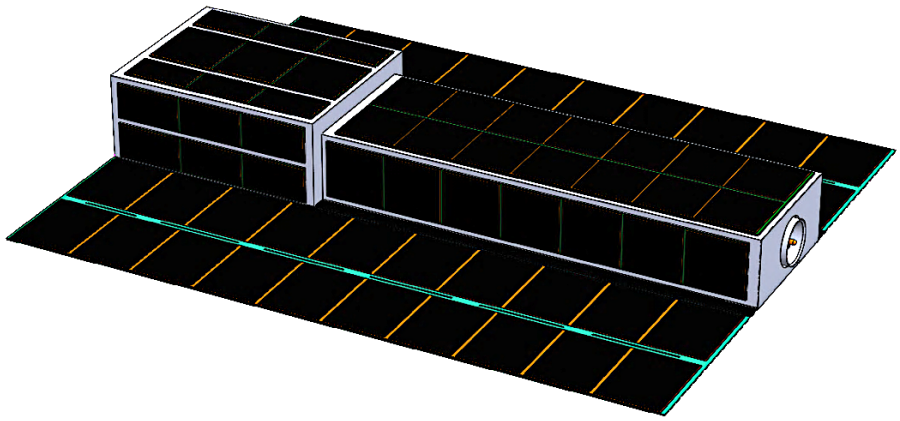

Figure 2. Volume envelope of conceptual satellite design. Ram inlet and flow compression are envisioned in the forebody at the left with an EP thruster contained in the afterbody along with other bus components. The backward-facing step of the forebody provides drag reduction for the afterbody.

3.2 Conceptual Design CAD Layout

Estimated sizing information from brassboard thruster hardware [Zimmerman, 2025] and volume estimates of a flow compression system, thruster system and satellite bus hardware, define a volume envelope for an EP-equipped VLEO satellite. **Figure 2** shows the volume envelope and **Figure 3** provides a top view diagram with estimated sizes. **Figure 2** shows solar panels hinged from the base of a rigid frame, providing support for the solar panels when folded into a stowed configuration for launch.

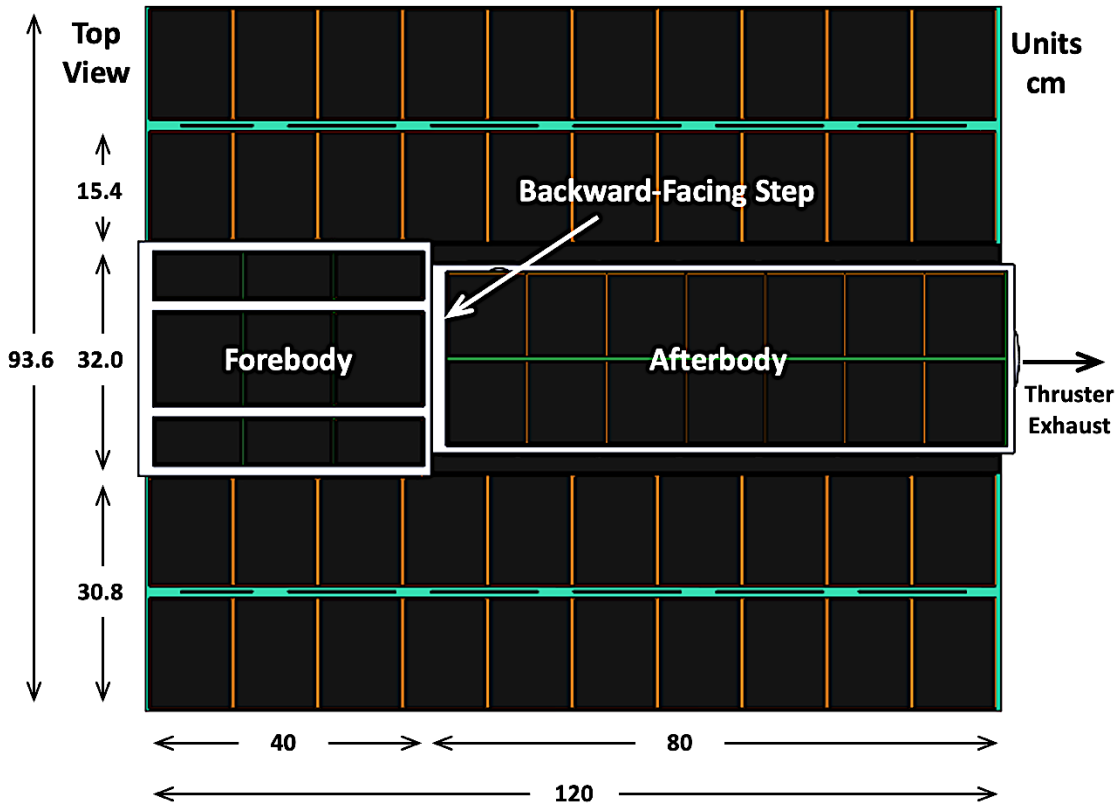

Figure 3. Top view of EP-equipped satellite. Forebody is towards the left of the image and thruster to the right side contained in the afterbody. Height of forebody is 16 cm (not shown). Height and width of afterbody are variable (discussed in Section IV) and depend on the height of the backward-facing step.

IV. Satellite Drag Calculation

4.1 Free Molecular Flow Theoretical Drag Estimates for Elongated Box Satellite

The drag on a satellite in VLEO where rarefied free molecular flow (FMF) effects are critical can be estimated by analytic methods [Sentman, 1961(a,b); Sentman, 1969], assuming fully diffuse accommodation coefficients and basic geometric shapes such as flat plates, cylinders, cones (including blunt end cones), and spheres. From the Sentman derivation {see Section III, Eqs. (3) and (8) in Sentman [1961a]}, the exact analytic solution for the coefficient of axial force imparted on a flat plate with two sides $C_{A,2sides}$ exposed to free molecular flow (e.g., deployed solar panels), and one side $C_{A,1side}$ exposed (e.g., body fixed panels) to the free molecular flow are, respectively:

$$C_{A,2sides} = \frac{A_{eff}}{A_{ref}}\left\{\left(2\cdot\cos\alpha\cdot\sin\alpha\cdot erf(\mathrm{S}\cdot\sin\alpha)\right)+\frac{2\cos\alpha}{S\sqrt{\pi}}e^{-S^2\sin^2\alpha}\right\} \tag{1}$$

and,

$$C_{A,1side} = \frac{A_{eff}}{A_{ref}}\left\{\left(\cos^2\alpha+\frac{1}{2S^2}\right)\left(1+erf(\mathrm{S}\cdot\cos\alpha)\right)+\frac{\cos\alpha}{S\sqrt{\pi}}e^{-S^2\cos^2\alpha}\right\} + \frac{A_{eff}}{A_{ref}}\left\{\sqrt{\frac{T_r}{T_i}}\left[\frac{\sqrt{\pi}}{2S}\cos\alpha\left(1+erf(\mathrm{S}\cdot\cos\alpha)\right)+\frac{1}{2\cdot S^2}e^{-S^2\cos^2\alpha}\right]\right\}, \tag{2}$$

where S is the speed ratio V_{sat}/c_m, α is the angle of attack with respect to the ram flow, V_{sat} is the satellite velocity, c_m is the most probable random speed $\sqrt{2RT_i}$ of the molecule, T_r is the reflected molecule temperature, T_i is the incident molecule temperature, A is the area of the surface impacted and A_{ref} is a reference area. Note that the equation for the case for two exposed sides considers a plate that is edge-on (parallel) to the flow, and the case for one exposed side is for a face-on plate (perpendicular) to the flow [Sentman, 1961a]. For an angle of attack of 0° achieved by zero pitch and yaw angles, these equations simplify for a two-sided panel to:

$$C_{A,2sides} = \frac{A_{eff}}{A_{ref}}\left\{\frac{2}{\sqrt{\pi}S}\right\} \tag{3}$$

and for a one-sided panel,

$$C_{A,1side} = \frac{A_{eff}}{A_{ref}}\left\{\left(1+\frac{1}{2S^2}\right)\left(1+erf(S)\right)+\frac{1}{S\sqrt{\pi}}e^{-S^2}+\sqrt{\frac{T_r}{T_i}}\left[\frac{\sqrt{\pi}}{2S}\left(1+erf(S)\right)+\frac{1}{2\cdot S^2}e^{-S^2}\right]\right\} \tag{4}$$

The effective drag (axial force) F_D on the satellite is the summation of forces over all surfaces:

$$F_D = q\sum_i A_i C_{A,i}\,, \tag{5}$$

where q is the dynamic pressure at the specified altitude. The drag force can then be readily estimated analytically for a satellite box (each face of the box being single sided) with two deployable solar arrays (with two sides).

As a first estimate, a simple elongated box satellite was analyzed with a 16 cm x 32 cm x 120 cm body having 4 solar panels (double-deployable panels with a hinge between pairs) that were assumed to be 15.4 cm x 120 cm, i.e., approximately the size of one of the sides of the satellite illustrated in **Figures 1 – 3**. An altitude of 210 km was chosen and using the MSISE-90 atmospheric model a number density of $5.22\text{x}10^{15}$ molecules/cm^3 was estimated. For simplicity and comparison to direct simulation Monte Carlo (DSMC) simulations, pure N_2 was assumed resulting in a dynamic pressure of $7.34\text{x}10^{-3}$ N/m^2. **Table 1** lists the analytically computed drag and drag/unit area on each satellite face at 0° angle of attack. Another parameter of interest is the effective total coefficient of drag based upon the ram-facing front face:

$$C_{D,eff} = F_D/qA_{ram}. \tag{6}$$

For this simple elongated box satellite, $C_{D,eff} = 4.884$, which is considerably higher than the classic value of 2.2 for a LEO satellite [Cook, 1965], a result of the significant drag imparted by the elongated satellite sides and the deployed solar panels, **Table 1**. Of the total drag of 1.836 mN, the drag of the front face (0.790 mN) is 76% of the drag of the side and deployable panels (1.046 mN). The effective C_D of the side and deployable panels without the front ram (or back) face is $C_{D,panel} = F_{D,panel}/qA_{panel} = 0.001046$ N / (0.00734 N/m^2 x 1.892 m^2) = 0.0753. It is significant that while the effective value of $C_{D,panel}$ is small, the imparted drag is large because of the large, exposed surface area.

Table 1. Analytically computed drag and drag/unit area on each satellite face at α=0°, Eqs. (3–5).

Satellite Feature	Area, effective (m^2)	C_A x (A_{ref}/A_{eff})	Drag (mN)	% of Full Satellite Drag	Drag/area (mN/m^2)
Front (ram) Face	0.0512	2.1026	0.7904	43.1	0.0154
Side (Starboard)	0.1920	0.0541	0.0763	4.2	0.3974
Side (Port)	0.1920	0.0541	0.0763	4.2	0.3974
Side (Top)	0.3840	0.0541	0.1526	8.3	0.3974
Side (Bottom)	0.3840	0.0541	0.1526	8.3	0.3974
Back Face	0.0512	0.0000	0.0000	0.0	0.0000
Deployed Panels	0.7392	0.1083	0.5876	32.0	0.7949
Full Satellite			1.836	100.0	

Note that the speed ratio $S = V_{sat}/c_m$ is dependent on the local atmospheric temperature, increasing drag during periods of high solar activity and reducing drag diurnally in shadowed regions of the orbit.

While there is little that can be done to reduce ram drag and drag from the solar panels that provide most of the power for the EP thruster, these analytic results indicate that the drag from the elongated satellite sides in this example contributes 25% of the total satellite drag. This suggests that creation of a backward-facing step may reduce drag from the elongated sides. There is no known study that provides this answer for rarefied gas flow; therefore, a basic science effort was undertaken to determine the effect, **Section 4.2**.

4.2 DSMC Drag

While drag can be estimated by analytic methods [Sentman, 1961a] for satellites composed of basic geometric shapes, **Section 4.1**, these methods fail with more complex configurations such as a backward-facing step between the air intake forebody and the thruster afterbody (**Section III**). As such, a particle-in-cell plus direct simulation Monte Carlo (PIC-DSMC) code called CHAOS [Jambunathan, 2018; Nuwal, 2022], developed at the University of Illinois at Urbana-Champaign (UIUC), was utilized to calculate the reduction in drag with a backward-facing step in a representative VLEO rarefied gas flow.

For VLEO conditions, the CHAOS code was first validated against internal flow conditions for nitrogen molecules. The air intake for an airbreathing EP system may have capillary ducts to decrease inlet backflow. The capillary factors W_{in} and W_{out}, defined by the flow rate through the capillary duct inlet into a downstream plenum and the flow rate in the reverse direction [van Essen, 1976; Varoutis, 2008], are key factors for sizing and designing the system turbo-molecular pumps. However, previous studies of conductance in vacuum systems only obtained W_{in} when the inlet bulk velocity was zero. The mean free paths for gases at VLEO conditions are too large to allow calculations using continuum methods such as Navier-Stokes. The results were compared to various calculations, experiments, and simulations in the literature [van Essen, 1976; Steckelmacher, 1978; Varoutis, 2008; Li, 2013] and the W_{out} calculations from CHAOS were found to be in good agreement. These initial simulations provided validation of the CHAOS code for conditions appropriate to VLEO conditions.

4.2.1 Simulation Setup

To assess the drag that a satellite with a backward-facing step would experience in VLEO, the rarefied flow and drag was calculated using CHAOS for a simple box shape and results were compared to exact analytic calculations. Particle collisions were modeled using the no time counter (NTC) method and variable hard-sphere (VHS) model. Both nitrogen molecules and atomic oxygen were modeled for these drag calculations. Gas species parameters used in this work are shown in **Table 2** [Xiao, 2014]. The inflow conditions at the calculation domain boundary used in this simulation are shown in **Table 3**. The box configuration initially tested was a 2D geometry and the resulting drag per unit area for a one-sided exposed flat side was computed to be $0.3993\ \mathrm{mN/m^2}$, within 0.5% of the analytic value of $0.3974\ \mathrm{mN/m^2}$, **Table 1**. While this error could be reduced further by using a significantly larger domain and grid density, the 0.5% error was viewed as sufficiently accurate, and serves as initial validation of the CHAOS code for VLEO conditions.

Table 2. Gas species parameters used for CHAOS simulations.

Parameters	Nitrogen molecule (N_2)
Mass (kg)	4.65×10^{-26}
Diameter (m)	4.17×10^{-10}
Viscosity index	0.74

Table 3. Flow conditions used for CHAOS simulations.

Altitude (km)	210
Number density, n_o (m^{-3})	5.22×10^{15}
Density, ρ (kg/m^3)	2.43×10^{-10}
Dynamic Pressure, q (N/m^2)	7.34×10^{-3}
Gas species	N_2
Flow velocity distribution	Half-Maxwellian
Collision Cross Section of N_2 molecule, σ (m^2)	4.3×10^{-19}
Mean free path = $(n_o\sigma)^{-1}$ (m)	446
Knudsen number (for characteristic length L = 1 m)	446
Bulk velocity, V_{sat} (m/s)	7,777
Temperature, T_o (K)	938
Mean thermal velocity of N_2 (m/s)	842

Drag reduction with a backward-facing step was then quantified with the CHAOS code. The satellite geometry drag was calculated in both 2D (**Figure 4**) and 3D (**Figure 5**) geometries. The backward-facing step appears 40 cm downstream from the front face (leftmost x-plane), and two step heights, d_{step} of 2 cm and 4 cm, were tested. The free stream comes from the left-hand side as seen from the satellite. The satellite is 120 cm long along the x-axis, 16 cm high along the y-axis, and 32 cm wide along the z-axis. The wall reflection model is a fully diffuse reflection model, in which it is assumed that molecules will reflect diffusely with complete energy accommodation [Hedahl, 1995]. The wall temperature is set at 273 K.

Since CHAOS is a three-dimensional code, the z-axis thickness is set to a short distance (1.875 cm), and a symmetry boundary condition is used on the z-direction boundaries for the 2D calculation to save computational costs. This simulation is essentially collisionless because the mean free path is in the order of 100 m, and the satellite characteristic length is 1 m. Calculation geometry sizes are (DX, DY, DZ) = (256 cm, 32 cm, 32 cm).

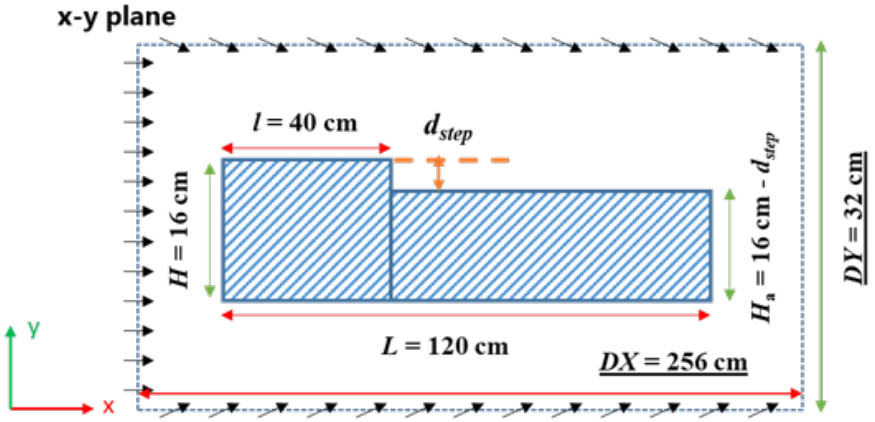

Figure 4. Backward-facing step (2D geometry).

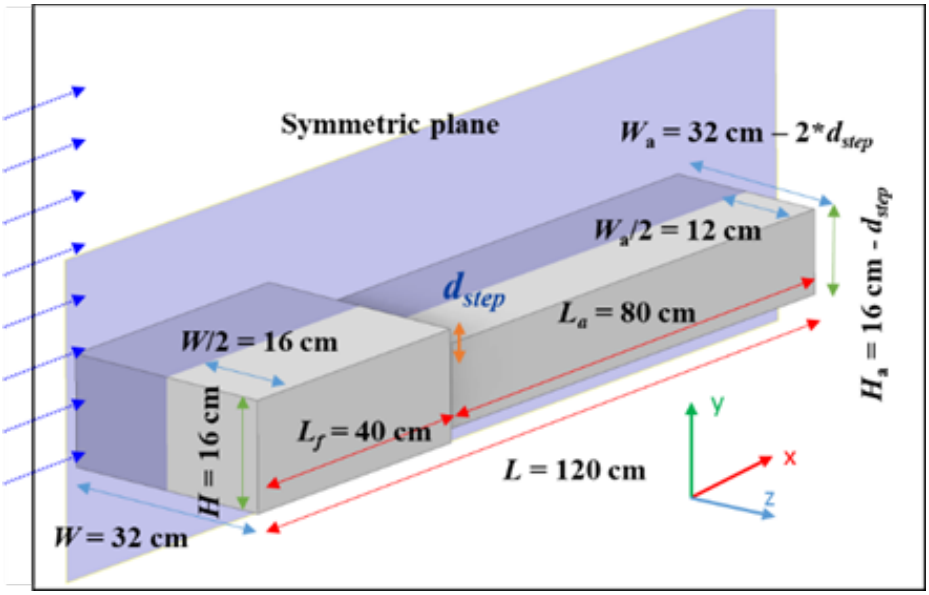

Figure 5. Backward-facing step (3D geometry).

To obtain the dependency of drag on step location, each side surface is divided into 60 bins. The drag on each face on the satellite is obtained by directly sampling the particle momentum difference, Δp_p. First, Δp_p is calculated when a particle hits the satellite wall as $\Delta p_p = m(v_a - v_b)$, where m is the mass of gas particles, v_a is velocity after reflection, and v_b is velocity before reflection. The total momentum to the wall is calculated as $\Delta p_w = \sum_i^n (-\Delta p_{p,i})\, F_{\text{num}}$, where n is the number of particles that hit the wall, and F_{num} is the real-computational particle weight ratio. Finally, the x-direction drag force on each wall is obtained as $F = \Delta p_{w,x}/\Delta t$, where Δt is the computational timestep.

In terms of the numerical parameters related to the simulations, a time step of $\Delta t = 0.1\ \mu s$ was used. The simulations were run for 20,000 timesteps and sampled for 60,000 additional time steps. The ratio of real to simulated particles F_{num} was 1.0×10^8 and the total number of computational particles was $\sim 3.2 \times 10^6$ for 2D cases and $\sim 20 \times 10^6$ for 3D cases.

4.2.2 CHAOS Results for Backward-Facing Step

The effect of step size was compared for the 2D and 3D cases. **Figure 6a** shows drag normalized by the area of the sampled bin in the top plane, where the bin spans the entire width in the z-direction, and each bin represents an average value in the z-direction. In all cases, the drag decreases to zero at the step location of 0.4 m, and then slowly recovers. This figure shows no significant difference between the 2D and 3D calculations for step sizes smaller than 4 cm, indicating that the relative size of the steps investigated are small enough for the satellite width of 32 cm and that the 3D effect of the side flow from the z-direction is small enough as to be insignificant. Next, comparing the step sizes, the drag recovering distance is longer for the 4 cm case than for the 2 cm case, showing that drag reduction increases with step size as expected.

Figure 6b shows the drag each face receives as a function of distance from the front face in the 3D case. Similarly to **Figure 6a**, each bin represents the average value of the flow perpendicular to the face. First, the drag received by the bottom face of the step does not change, while for the side and top faces, the drag decreases as the step height d_{step} increases, as shown in **Figure 6a**. In this computational geometry, in which the width and height are different (see **Figure 5**), the three-dimensional effect is smaller when the step is small, as shown in the 2 cm case (brown and purple). On the other hand, when the step is larger, as shown in the 4 cm case (green and orange), a difference in drag between the side and top surfaces is observed.

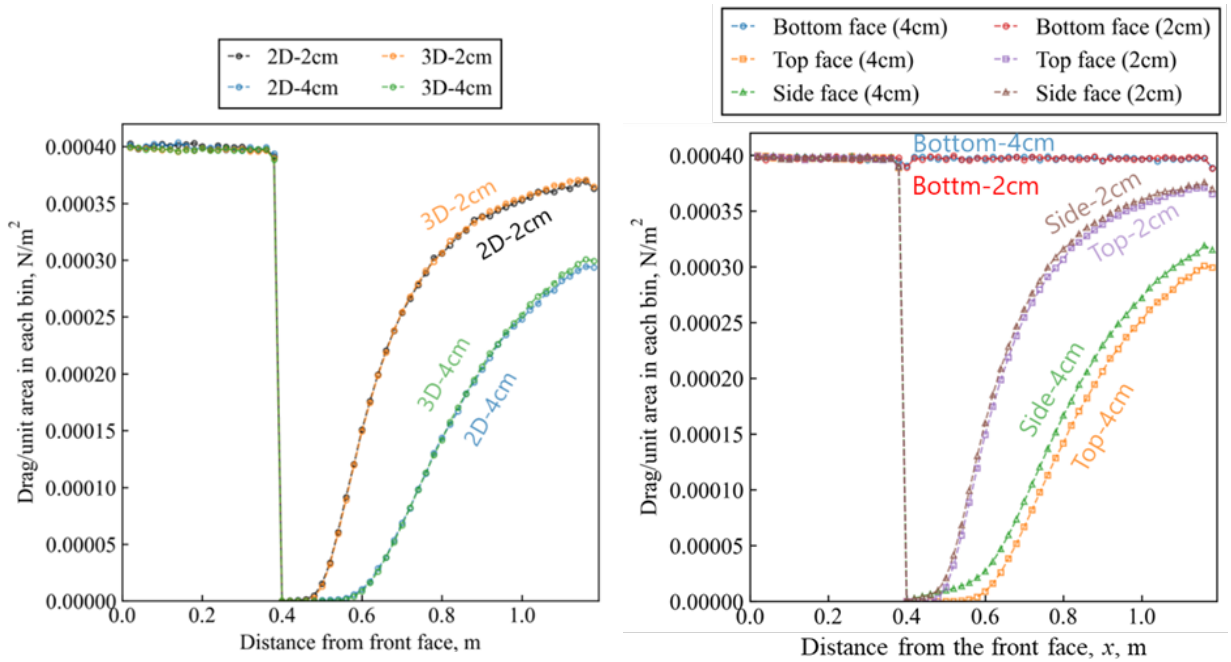

(a) 2D vs 3D, top face, varied step size **(b) 3D calculation for bottom, top and sides**

Figure 6. Drag per unit area versus distance from the ram face.

Finally, drag/panel area computed for the 2D cases is shown in **Table 4** for a bottom face without a step and a top face with different step sizes. Comparing the bottom and top faces, the reduction in average drag/area with and without the step is 22% for the 1 cm step, 40% for the 2 cm step, and 66% for the 4 cm step.

Table 4. Average drag/unit area on top and bottom faces of a satellite afterbody having 1 cm, 2 cm, and 4 cm steps as computed with the DSMC CHAOS code for a 2D geometry.

Values	d_{step}	Bottom face (w/o step)	Top face (w/ step)	Average Fraction Over 80 cm Aft Body	Average % Reduction Over 80 cm Aft Body
Average	1 cm	0.399	0.313	0.784	21.6
Drag/area	2 cm	0.399	0.241	0.604	39.6
(mN/m^2)	4 cm	0.399	0.134	0.337	66.3

In summary, the following key findings were established using the CHAOS code:

- Quantitative DSMC calculations were used to obtain the drag of a VLEO satellite with a BFS.
- For steps of 4 cm or less, the drag at the top face is well predicted by 2D calculations.
- For 3D geometries with different widths and heights, the larger the step, the greater the difference in drag at the side and top faces.
- The larger the step, the smaller the drag on the 80 cm top aft face along the direction of satellite travel, with a 66% drop in drag for a 4 cm step.

4.3 Free Molecular Flow Theoretical Drag Estimates for Satellite with Backward-Facing Step

It is now possible to make an estimate of the impact of drag on the satellite illustrated in **Figures 1 – 3** having a BFS on the top and sides, resulting from an afterbody EP system with cross section smaller than the forebody cross section. The simple elongated box satellite of **Table 1** is split into two boxes having a 16 cm x 32 cm x 40 cm forebody and a 14 cm x 28 cm x 80 cm afterbody (for a 2 cm backward-facing step), as illustrated in **Figure 6**. The same sized deployable solar panels are assumed as in **Table 1**. Using values for the average drag/unit area over the 80 cm afterbody from **Table 6**, the drag on this satellite shape can be analytically computed, **Table 5**. Comparing **Tables 1 and 5** shows that the drag on the basic satellite shape decreases from 1.836 mN to 1.727 mN for the satellite with a 2 cm backward-facing step on the top and starboard/port sides, a 5.9% drag decrease.

Table 5. Analytically computed drag and drag/unit area on each face of the 40 cm fore body and an 80 cm aft body with a 2 cm backward-facing step on top and sides. Angle of attack α=0°, Eqs. (3–5). Note: $C_A(A_{ref}/A_{eff})$ values for the aft body are adjusted according to values in Table 6.

Body	Satellite Feature	Area, effective, exposed (m^2)	$C_A(A_{ref}/A_{eff})$	Drag (mN)	% of Full Satellite Drag	Drag/area (mN/m^2)
Fore	Front (ram) Face	0.0512	2.1026	0.7904	45.8	15.44
Fore	Side (Starboard)	0.0640	0.0541	0.0254	1.5	0.397
Fore	Side (Port)	0.0640	0.0541	0.0254	1.5	0.397
Fore	Side (Top)	0.1280	0.0541	0.0509	2.9	0.397
Fore	Side (Bottom)	0.1280	0.0541	0.0509	2.9	0.397
Fore	Back Face	0.0120	0.0000	0	0.0	0.0000
Aft	Front (ram) Face	0.0000	2.1026	0	0.0	0.0000
Aft	Side (Starboard)	0.1120	0.0326	0.0268	1.6	0.240
Aft	Side (Port)	0.1120	0.0326	0.0268	1.6	0.240
Aft	Side (Top)	0.2240	0.0326	0.0537	3.1	0.240
Aft	Side (Bottom)	0.2240	0.0541	0.0890	5.1	0.397
Aft	Back Face	0.0392	0.0000	0		0
---	Deployed Panels	0.7392	0.1083	0.5876	34.0	0.795
	Full Satellite			1.727	100.0	

Using a similar process, it is possible to compute analytically the drag on multiple configurations and different atmospheric conditions. **Table 6** lists realistic atmospheric conditions at 210 km taken from the MSISE-90 data base [Rajendra, 2001; Picone, 2002]**,** with exosphere temperature T_{exo} = 1000 K and temperature at altitude T(210 km) = 938 K. **Table 7** lists different configurations and the corresponding drag. The backward-facing step does reduce overall satellite drag as much as 7.6% with the 4 cm step on the top face. Lastly, the MSISE-90 atmospheric conditions (**Table 6**) are more favorable than the simplified N_2-only conditions (**Table 3**). The effective drag coefficient on the satellite is computed from Eq. (6).

Table 6. Atmospheric conditions taken from MSISE-90 data base for T_{exo} = 1000 K.

Altitude (km)	210
Number density, n_o (m^{-3})	5.45×10^{15}
Gas species	O, N_2, N, O_2, He, H, and Ar
Average Molecular Weight (g/mole)	20.85
Density, ρ (kg/m^3)	1.89×10^{-10}
Dynamic Pressure, q (N/m^2)	5.71×10^{-3}
Temperature, T_o (K)	938
Collision Cross Section of N_2 molecule, σ (m^2)	4.3×10^{-19}
Mean free path = $(n_o\sigma)^{-1}$ (m)	427
Knudsen number (for characteristic length L = 1 m)	427
Bulk velocity, V_{sat} (m/s)	7777
Most probable random molecular speed, c_m (m/s)	865
Speed ratio, S	8.99

Table 7. Analytically computed drag for different satellite body configurations, some with a 40 cm forebody and an 80 cm afterbody with different sizes of backward-facing steps on top and starboard/port sides. The "Simple" configuration is an elongated box with deployable solar panels and no BFS (Table 1). Calculations are shown for circular 210 km orbits and two different atmospheric conditions. Dynamic pressure q (mN/m^2) is 7.34 and 5.71 for the atmospheric conditions given in Tables 3 and 6, respectively.

Configuration Body Type	Backward-Facing Step Size (cm)	Atmospheric Conditions	Ram Frontal Area (m^2)	Satellite Drag, mN	Fraction of Simple Config. Drag (%)	Effective Drag Coeff. $C_{D,eff}$
Simple (Table 1)	0	Simplified (Table 3)	0.0512	1.836	100	4.88
Fore+Aft w/ BFS (Table 5)	2 cm top & sides	Simplified (Table 3)	0.0512	1.727	94.1	4.59
Fore+Aft w/ BFS	4 cm top 2 cm sides	Simplified (Table 3)	0.0512	1.696	92.4	4.51
Fore+Aft w/ BFS	4 cm top 2 cm sides	MSISE-90 (Table 6)	0.0512	1.435	78.2	4.91

V. Thruster Option for VLEO Satellite

Vehicle drag calculations show that frontal drag is a significant fraction of total drag (**Tables 1 and 5**). The reduced propellant requirement and inlet size of high exhaust velocity propulsion therefore reduces the power requirement, solar panel area and the corresponding panel drag. For this reason, several investigations have been performed of air-breathing thrusters with high exhaust velocity propulsion mechanisms, including ion, Hall, inductive and electromagnetic. [Burton, 1983, Haas, 2000; Nakagawa, 2003; Hruby, 2004; Lotz, 2013; Shabshelowitz, 2014; Barral, 2015; Romano, 2017; Romano, 2019; Andreussi, 2022; Hruby, 2022; Herdrich, 2024; Zimmerman, 2025]. Because purely thermal acceleration is inadequate for the VLEO application, all of these EP systems have in common the ionization of air and the acceleration of air ions by an axial electric field.

An EP option that has several advantages in VLEO is the pulsed magnetoplasmadynamic thruster (MPDT) system. Complete (100%) ionization and $\vec{j} \times \vec{B}$ acceleration of the collected air is generated by a pulsed megawatt discharge, as opposed to lower power propulsion systems that achieve partial ionization with a steady-state discharge. Because accelerated ions are imbedded in a charge-neutral plasma, a charge neutralizer is not required. In addition, a pulsed system is inherently throttleable, allowing for large variations in atmospheric density, air composition and vehicle drag. The MPD thrust acceleration mechanism has been amply described by extensive research on self-field electromagnetic discharges and gas-fed pulsed plasma thrusters since the 1960s [Jahn, 1968; Malliaris, 1972; Burton, 1983; Uematsu, 1985; Ziemer, 1999a; Ziemer, 1999b; Choueiri, 2001; Ziemer, 2001a; Ziemer, 2001b; Cooley, 2005; Cooley, 2008; Burton, 2023; Burton, 2025b], along with in-space thruster operations [Toki, 2000]. Further, MPDTs have performed successfully with many gases including N_2 [Burton, 1983], O_2 [Uematsu, 1985], and N_2:O_2 mixtures [Zimmerman, 2025] as required for VLEO operations.

High specific impulse (high exhaust velocity) for the pulsed MPD thruster propulsion system is desired and is expected to be 3000 – 4000 seconds (U = 30-40 km/s). This takes advantage of the increasing efficiency of the MPDT with exhaust velocity, reducing power requirements, and also of the reduced mass flow requirement and therefore the reduced inlet drag at high I_{sp}, again reducing the power requirement. Note that prior experimental data [Burton, 1983; Zimmerman, 2025] show that exhaust velocities of 30-40 km/s for N_2-fed and N_2:O_2-fed MPDTs have been achieved.

Based upon the drag of 1.44 mN computed for the VLEO satellite at 210 km, **Table 7** (for the 4 cm backward facing step and MSISE-90 atmosphere), desired characteristics of an MPDT based upon prior experimental data [Burton, 1983] are listed in **Table 8**.

Table 8. Preliminary MPDT characteristics for the VLEO satellite.

Feature	Description
Thrust mechanism	Coaxial electromagnetic $\left(\vec{j} \times \vec{B}\right)$
Ionization method	Electron impact in megawatt discharge
Thruster Efficiency, η_t	~ 40% exhaust energy/pulse energy
Exhaust Velocity, U_e	40 km/s
Nominal Pulse Rate	0.2 Hz (1 pulse every 5 seconds)
Pulse momentum (impulse bit)	> 7.2 mN-s (= 1.44 mN / 0.2 Hz)

VI. Conclusion

A satellite with a backward-facing step for drag reduction and air-breathing MPD propulsion, may be equipped with a larger ram area forebody and smaller afterbody. Free molecular flow drag effects were calculated for the extended satellite body. Significant basic science implications of this work for VLEO satellites are:

1) DSMC calculations using the UIUC CHAOS code for the drag on a satellite side panel showed good agreement with the analytic methods of Sentman to within 0.5%, consistent with the assumed calculation domain and grid density.
2) Basic DSMC simulations of a backward-facing step predict significant reductions in satellite side panel drag, with a reduction of as much as 66% for a 4 cm step over an 80 cm length.
3) Satellite drag calculations indicate a significant 8% reduction in overall drag for a design with elongated body and a backward-facing step.
4) The drag incurred by airbreathing VLEO EP propulsion systems such as the MPD thruster with an oversized forebody can be partially offset by a satellite design incorporating a backward-facing step.

Acknowledgments

This research was developed with funding from the Defense Advanced Research Projects Agency (DARPA) on Contract # N66001-22-C-4011. The views, opinions and/or findings expressed are those of the authors and should not be interpreted as representing the official views or policies of the Department of Defense or the U.S. Government. The authors wish to thank Stephen Forbes and Aaron Esposita for their guidance and support.

References

Andreussi T, *et al.*, "Characterization of an Atmospheric Propellant-fed Hall Thruster as a VLEO Simulator," *37th Int. Electric Propulsion Conf.*, IEPC-2022-435, June 19-23, 2022.

Barral, *et al*., "Conceptual Design of an Air-Breathing Electric Propulsion System," *34th International Electric Propulsion Conference*, IEPC-2015-271, 2015.

Burton, R.L., Clark, K.E., and Jahn, R.G., "Measured Performance of a Megawatt MPD Thruster," *J. Spacecraft*, Vol. 20, No. 3, 1983. https://doi.org/10.2514/3.25596

Burton, R.L. and D.L. Carroll, "Simplified Plasmadynamics Model of a Coaxial Self-Field Plasma Accelerator," *J. of Propulsion and Power*, Vol. 39 (4), 511-523, 2023. https://doi.org/10.2514/1.B38923.

Burton, R.L. and D.L. Carroll, "Fundamental Characteristics of VLEO Satellites with Airbreathing Propulsion," *Acta Astronautica*, Vol. 237, 371-380, 2025a. https://doi.org/10.1016/j.actaastro.2025.09.001

Burton R L, Carroll D L, and Zimmerman J W, "Magnetoplasmadynamic Thruster with Reverse Polarity and Tailored Mass Flux," U.S. Patent No. 12,309,909, 2025b.

Choueiri, E.Y. and J.K. Ziemer, "Quasi-Steady Magnetoplasmadynamic Thruster Performance Database," *J. of Propulsion and Power*, Vol. 17, No. 4, pp 967-976, 2001. https://doi.org/10.2514/2.5857

Cooley J E and Choueiri E Y, Fundamentals of discharge initiation in gas-fed pulsed plasma thrusters. In *29th Int. Electric Propulsion Conference*, Princeton, NJ, IEPC-2005-153, 2005.

Cooley J E and Choueiri E Y, "Threshold Criteria for Under-voltage Breakdown," *J. Applied Physics,* Vol. 103, 093305, May 2008. https://doi.org/10.1063/1.2913196

Cook G E, "Satellite Drag Coefficients," *Planetary and Space Science*, vol. 13, pp. 929-946, 1965.

Crandall P and Wirz R E, "Air-Breathing Electric Propulsion Spacecraft Performance and Aerodynamic Maneuverability," *37th Int. Electric Propulsion Conf.*, IEPC-2022-444, June 19-23, 2022.

Feldman M S and Spektor R, "Basic Analysis of an Air Breathing Electric Propulsion Concept," *37th Int. Electric Propulsion Conf.*, IEPC-2022-468, June 19-23, 2022.

Giannetti V, Ferrato E, and Andreussi T, "On the critical parameters for feasibility and advantage of air-breathing electric propulsion systems," *Acta Astronautica*, Vol. 220, pp. 345-355, 2024. https://doi.org/10.1016/j.actaastro.2024.04.042

Haas J M and Gallimore A D, "An Investigation of Internal Ion Number Density and Electron Temperature Profiles in a Laboratory-Model Hall Thruster," *36th Joint Propulsion Conference*, AIAA-00-3422, 2000.

Hedahl, M. O., "Comparisons of the Maxwell and CLL Gas/Surface Interaction Models Using DSMC," Technical Reports: Langley Aerospace Research Summer Scholars, vol. Part 1, no. January, pp. 285–294, Jan. 1995.

Herdrich G, Papavramidis K, Maier P, Skalden J, Hild F, Beyer J., Pfeiffer M, Fugmann M, Klinker S, Fasoulas S, Souhair N, Ponti F, Walther M, Wiegand A, Walpot L, Duesmann B, Borras E B, Roberts P C E, and Crisp N G, "System design study of a CLEO satellite platform using the IRS RF helicon-based plasma thruster," *Acta Astronautica*, Vol. 215, pp. 245-259, 2024. https://doi.org/10.1016/j.actaastro.2023.11.009

Hruby V, *et al*., "Air Breathing Electrically Powered Hall Effect Thruster," U.S. Patent No. US 6,834,492, B2 Dec. 28, 2004.

Hruby V, Hohman K, and Szabo J, "Air Breathing Hall Effect Thruster Design Studies and Experiments," *37th Int. Electric Propulsion Conf.*, IEPC-2022-446, June 19-23, 2022.

Jahn R G, *Physics of Electric Propulsion*, Chapter 8, McGraw-Hill, New York, 1968.

Jambunathan, R. and D. A. Levin, "CHAOS: An octree-based PIC-DSMC code for modeling of electron kinetic properties in a plasma plume using MPI-CUDA parallelization," *J. Comput. Phys*., vol. 373, pp. 571–604, Nov. 2018.

Li, Y., X. Chen, L. Wang, L. Guo, and Y. Li, "Molecular flow transmission probabilities of any regular polygon tubes," Vacuum, vol. 92, pp. 81–84, Jun. 2013.

Lotz, B., "Plasma physical and material physical aspects of the application of atmospheric gases as a propellant for Ion-Thruster of the RIT-Type," doctoral thesis, University of Giessen, 2013.

Malliaris A C, John R R, Garrison R L, and Libby D R, “Performance of Quasi-Steady MPD Thrusters at High Powers,” *AIAA J*., Vol. 10, No. 2, pp. 121-122, 1972.

Mehta, P.M., et al., “Satellite drag coefficient modeling for thermosphere science and mission operations,” *Adv. Space Res*., Jun. 2022.

Nakagawa T, *et al*., "Experimental Investigation of a Hall Thruster using Oxygen as the Propellant," *J. of the Japan Society for Aeronautical and Space Sciences*, Vol. 51, No. 598, pp. 606-612, 2003.

Nuwal, N., R. Jambunathan, and D. A. Levin, “Kinetic Modeling of Spacecraft Surfaces in a Plume Backflow Region,” *IEEE Trans. Plasma Sci. IEEE Nucl. Plasma Sci. Soc*., vol. 48, no. 12, pp. 4305–4325, Dec. 2020.

Picone J M, Hedin A E, Drob D P, and Aikin A C, “NRLMSISE-00 empirical model of the atmosphere: Statistical comparisons and scientific issues,” *J. Geophysical Research*, Vol. 107, No. A12, 1468, 2002.

Rajendra P P and Kuga H K, “An Evaluation of Jacchia and MSIS 90 Atmospheric Models with CBERS Data,” *Acta Astronautica*, Vol 48, No. 5-12, pp. 579-588, 2001.

Romano F, *et al.*, “Literature Review of ABEP Systems,” Project Discoverer Report, Horizon 2020, 6 March 2017.

Romano F, *et al.*, “Inductive Plasma Thruster (IPT) for an Atmosphere-Breathing Electric Propulsion System: Design and Set in Operation,” *36th International Electric Propulsion Conference*, IEPC-2019-A-488, 2019.

Sentman, L.H., “Free Molecule Flow Theory and its Application to the Determination of Aerodynamic Forces,” Lockheed Missiles and Space Co., LMSC Tech. Rep. 448614, 1961a.

Sentman, L.H., “Comparison of the Exact and Approximate Methods for Predicting Free Molecule Aerodynamic Coefficients,” *ARS Journal*, pp. 1576-1579, Nov. 1961b.

Sentman, L.H. and Karamcheti, K., “Rarefied Flow Past a Sphere,” *AIAA Journal*, vol. 7, no. 1, pp. 161-163, 1969.

Shabshelowitz, A., Gallimore, A. D and Peterson, P., "Performance of a Helicon Hall Thruster Operating with Xenon, Argon, and Nitrogen," *J. Propulsion and Power*, Vol. 30, No 3, 664, 2014.

Steckelmacher, W., “The effect of cross-sectional shape on the molecular flow in long tubes,” *Vacuum*, vol. 28, n. 6/7 pp. 269-275, 1978.

Tisaev, M., N. Baresi, A. Lucca Fabris, E. Ferrato, C. Paissoni, V. Giannetti, and T. Andreussi, “Flight envelope and in-orbit control analysis for an air-breathing electric propulsion spacecraft,” *37th International Electric Propulsion Conference Massachusetts Institute of Technology, Cambridge, MA, USA June 19-23, 2022*, IEPC-2022-455, 2022.

Toki, K., Shimizu, Y. and Kuriki, K., "On-Orbit Demonstration of a Pulsed Self-Field Magnetoplasmadynamic Thruster System," *J. Propulsion and Power*, Vol. 16, No. 5, 880, 2000. https://doi.org/10.2514/2.5655

Uematsu, K., Morimoto, S. and Kuriki, K., "MPD Thruster Performance with Various Propellants," *J. Spacecraft and Rockets*, Vol. 22, No. 4, pp 412-416, 1985. https://doi.org/10.2514/3.25766

van Essen, D. and W. C. Heerens, “On the transmission probability for molecular gas flow through a tube,” J. Vac. Sci. Technol. B Nanotechnol. Microelectron., vol. 13, no. 6, pp. 1183–1187, Nov. 1976.

Varoutis, S., D. Valougeorgis, O. Sazhin, and F. Sharipov, “Rarefied gas flow through short tubes into vacuum,” J. Vac. Sci. Technol. A, vol. 26, no. 2, pp. 228–238, Mar. 2008.

Xiao, H., Y. Shang, and D. Wu, “DSMC simulation and experimental validation of shock interaction in hypersonic low-density flow,” *Scientific World Journal*, vol. 2014, p. 732765, Jan. 2014.

Ziemer J K, Choueiri E Y, *et al.*, "Is the Gas-Fed PPT an Electromagnetic Accelerator? An Investigation using Measured Performance," *35th Joint Propulsion Conf.*, AIAA Paper 99-2289, 1999a.

Ziemer J K, Choueiri E Y, and Birx D, “Comparing the performance of co-axial and parallel-plate gas-fed PPTs,” *26th International Electric Propulsion Conf.*, Kitakyushy, Japan, IEPC-99-209, 1999b.

Ziemer J K, “Performance Scaling of Gas-Fed Pulsed Plasma Thrusters,” Ph.D. Dissertation, Princeton University, 2001a.

Ziemer J K and Choueiri E Y, “Scaling laws for electromagnetic pulsed plasma thrusters,” *Plasma Sources Science and Technology*, 10:395-405, 2001b. https://doi.org/10.1088/0963-0252/10/3/302

Zimmerman J W, Burton R L, Fox R T, and Carroll D L, Broemmelsiek R J, and Choueiri E Y, “Pulsed Magnetoplasmadynamic Propulsion for Airbreathing Satellites in Very Low Earth Orbit,” *J. Propulsion and Power*, Vol. 41, No. 6, pp. 810-813, 2025. https://doi.org/10.2514/1.B39990

10.2514/6.2026-0278.c1

Correction to AIAA-2026-0278

"Effect of a Backward-Facing Step on Drag of a VLEO Satellite"

David Carroll[1], Keita Nishii[2], Deborah Levin[2], Rodney Burton[1], Joseph Zimmerman[1], & Ryan Fox[1]

[1]CU Aerospace, L.L.C., Champaign, IL, 61822, USA

[2]University of Illinois at Urbana-Champaign, Urbana, IL, 61801, USA

Correction Notices:

1) Section 3.2, 1st sentence (p. 3), reference to [Zimmerman, 2024] should be [Zimmerman, 2025]
2) Section 4.3, sentence above Table 5 (p. 8), the value 1.863 mN should be 1.836 mN.